# Assessing the rate of crustal extension by 2D sequential restoration analysis: A case study from the active portion of the Malta Escarpment

Salvatore Gambino, Giovanni Barreca, Felix Gross, Carmelo Monaco, Marc-andré Gutscher, G. Ian Alsop

# Assessing the rate of crustal extension by 2D back-restoration analysis: a case study from the active portion of the Malta Escarpment.

Salvatore Gambino[1]*, Giovanni Barreca [1,2], Felix Gross[3,4], Carmelo Monaco [1,2,5] Marc-André Gutscher[6], Geoffrey Ian Alsop[7]

1) Department of Biological, Geological and Environment Sciences, University of Catania, Catania, Italy,
2) CRUST—Interuniversity Center for 3D Seismotectonics with Territorial Applications, Chieti, Italy,
3) Institute of Geosciences, Kiel University, Kiel, Germany,
4) Center for Ocean and Society, Kiel University, Germany, Kiel,
5) Istituto Nazionale di Geofisica e Vulcanologia, Osservatorio Etneo, Catania, Italy,
6) Laboratoire Géosciences Ocean, UMR6538 CNRS/University of Brest, Plouzané, France
7) Department of Geology & Geophysics, University of Aberdeen, Scotland, UK

**Corresponding Author (*)**
Salvatore Gambino
(salvatore.gambino@unict.it)

## Conflict of Interest

The authors declare that the research was conducted in the absence of any commercial or financial relationships that could be construed as a potential conflict of interest.

## Authors' contribution

SG: work planning, conceptualization, seismic data interpretation, data analysis and interpretation of results, review of literature, figures preparation, writing the initial draft and final version of the manuscript. GB: seismic data interpretation, data analysis and interpretation of results, review of literature, writing the initial

# Abstract

Tectono-stratigraphic interpretation and back-restoration modelling was performed over two high-resolution seismic profiles crossing the Western Ionian Basin of southern Italy. This analysis was undertaken in order to provide greater insights and a more reliable assessment of the deformation rate affecting the area. Offshore seismic profiling illuminates the sub-seafloor setting where a belt of recent/active faults slice across the foot of the Malta Escarpment, a regional-scale structural boundary inherited from the Permo-Triassic palaeotectonic setting. A sequential restoration workflow was established to back-deform the entire investigated sector with the primary aim of analysing the deformation history of the three major active faults affecting the area. Restoration of the tectono-stratigraphic model reveals how deformation rates evolved through time. In the early stage, the whole region experienced a significant deformation with the horizontal component prevailing over the vertical element. In this context, the three major faults contribute to only one third of the total deformation. The overall throw and extension then notably reduced through time toward the present day and, since the middle Pliocene, they were accommodated almost entirely by the three major normal faults. Unloading and decompaction indicate that when compared to the unrestored seismic sections, a revision and a reduction of roughly one third of the vertical displacement of the faults offset is required. This analysis ultimately allows us to better understand the seismic potential of the region.

**Keywords:** Malta Escarpment, seismic profile, Back-restoration, deformation rate.

## 1. Introduction

The back-restoration concept includes a wide range of methods (balanced cross-sections, back-stripping, structural restoration etc.), which are applied to validate structural interpretations or to recover deformation, subsidence or any other tectonic processes to be analysed. As seismic data is frequently not associated with well data, application of sequential back-restoration techniques

provides a powerful tool for the validation of structural interpretation (Lopez-Mir et al 2014;Jamaludin et al., 2015; Jitmahantakul et al., 2020), prediction of geometry at depth (Chamberlin 1910; Bally et al., 1966; Dahlstrom, 1969, 1970; White et al., 1986; Williams and Vann, 1987; Groshong,1990), and formulation of kinematic structural models (Suppe, 1983; Suppe and Medwedeff, 1990; Lopez-Mir et al., 2014). Restoration methods are usually based on 'balanced cross sections' as defined by Dahlstrom (1969) and Elliot (1983), through which all available data are analyzed to ensure they are geometrically plausible and geologically consistent. These methods usually follow reasonable assumptions about the pre-deformation setting and how rocks behave during deformation in a given tectonic environment (Dahlstrom, 1969).

Since the pioneering studies of Bally et al., (1966) and Dahlstrom (1969), balanced cross sections have been applied to section restoration for validation of structural interpretation and prediction of geometry at depth in both contractional (Hossack, 1979; Boyer and Elliot, 1982; Suppe, 1983; Suppe and Medwedeff, 1990) and extensional settings (Gibbs, 1983-1984;White et al., 1986, Williams and Vann, 1987; Groshong, 1990). More recently, greater computer power has led to a significant acceleration in section modelling and restorations (see Gratier et al., 1991; Egan et al., 1996; Maerten, 2007, among many others). In this case, structural balancing and horizon flattening were applied to rectify seismic interpretation in extensional settings (Jamaludin et al., 2015) or to validate 2D seismic interpretation and to calculate extension in various rift phases (Jitmahantakul et al., 2020).

Application of the above-mentioned methods represents a powerful approach for basin analysis and for detailing how deformation evolves through time. Step-by-step analysis of restored models provides further constraints for re-interpretation/validation of seismic profiles. In addition, the broad applicability of such methods allows them to be readily exported to various tectonic contexts (extensional, compressional or composite).

In this study, back-restoration methods were applied to analyse the rate of deformation of the extensional Malta Escarpment fault system (hereinafter MESC, see Fig. 1). The MESC is a former passive margin in the Western Ionian Basin that was reactivated by the Nubia-Eurasia plate convergence during Plio-Quaternary times (Casero et al., 1984; Argnani and Bonazzi, 2005). The reactivation of MESC involved the proximal part of a narrow sedimentary basin in the hanging-wall of the fault system, previously termed the 'turbidite valley' (see Gutscher et al., 2016 and Fig.1c), and its recent deformation is expressed by a belt of East-dipping extensional faults slicing across the lower slope of the MESC. Fault activity has led to the development of significant fault-scarps on the seafloor (Bianca et al., 1999; Argnani and Bonazzi, 2002, 2005) that sometimes exceed heights of 60m (see Gambino et al., 2021).

Assuming an age of 11.7 ka for the displaced seafloor, a slip rate > 5mm/yr is resolved for most of the considered extensional faults (Gambino et al., 2021). However, this value appears atypical when compared with general slip rates recorded in tectonic regimes (Galadini and Galli, 2000; Pizzi et al., 2002; Musumeci et al., 2014; Stemberk et al., 2019). This suggests that the height of seafloor scarps could be enhanced by sediment loading in the hanging-wall basin according to their thickening overtime, or may be produced by the cumulative effect of different kinds of tectonic and gravitational processes. Since fault slip rate is an essential parameter in seismotectonic analysis, and considering that the MESC is described by many authors as the seismogenic source for large historical earthquakes in the area (Piatanesi and Tinti, 1998; Bianca et al., 1999; Azzaro and Barbano, 2000; Argnani and Bonazzi, 2005; Argnani et al., 2012), we undertook a sequential restoration work-flow to model the Plio-Quaternary deformation rate of the reactivated northern sector of the MESC. The aim of this work is twofold, a) to reassess fault activity and associated slip rates through-time, and b) to discriminate which kind of processes operate to create basin deformation.

Sequential restoration was performed on a tectono-stratigraphic model developed from the interpretation of two high-resolution seismic profiles that transversally cross the MESC (see Gambino et al.; 2021; Gutscher et al., 2016). After time-to-depth conversion of the seismic profiles, several restoration methods such us sediment unloading and decompaction, isostatic adjustments, erosion restoration, structural restoration and unfolding of the horizons were performed in order to create a geologically consistent sequential restoration (see supplementary material). Accordingly, the present-day tectono-stratigraphic model was back-deformed step-by-step up to the initial stage of deformation. This process provides a more reliable estimation of the fault's deformation rate overtime, with significant implications for the seismic hazard of the investigated region.

## 2. Geological Setting

The 300 km-long Malta Escarpment is located about 20 km offshore Eastern Sicily and separates the thinned/oceanic crust of the Western Ionian Basin from the continental crust of the Pelagian block (Scandone et al., 1981; Fabbri et al., 1982; Casero et al., 1984, Fig.1a). It represents a rifting or spreading-like extensional relict inherited from the Permian-Triassic opening of Neo-Tethys (Şengör, 1979), and the subsequent Mesozoic spreading stage (Ben-Avraham and Grasso, 1991; Catalano et al., 2001). The MESC was reactivated during Quaternary times (Hirn et al., 1997; Bianca et al., 1999; Argnani and Bonazzi, 2005; Gambino et al., 2021) and is considered one of the most likely sources of major destructive earthquakes in the area over historical times, even though the actual localization of such events is still controversial (Piatanesi and Tinti, 1998; Bianca et al.,

1999; Azzaro and Barbano, 2000; Argnani and Bonazzi, 2005; Argnani et al., 2012; Gambino et al., 2021). This establishes the MESC as a crucial tectonic feature for the understanding of both the geodynamics of the central Mediterranean and the seismotectonics of the Western Ionian Basin and south-eastern Sicily.

To the East of the MESC, the Ionian Basin (Fig.1a) is interpreted by many authors as a remnant of the Mesozoic Tethys Oceanic crust (Carminati and Doglioni, 2005; Frinzon et al., 2011; Gallais, et al., 2013; Polonia et al., 2017; Speranza et al., 2012; Valenti, 2011), even though the actual nature of the underlying geology is still debated (Dellong et a., 2018). NW-directed subduction of the Ionian oceanic crust beneath the European plate resulted in the development of a large accretionary wedge in the Ionian Sea (the Calabrian accretionary wedge, see Gallais et al., 2012; Polonia et al., 2016). In contrast to the widespread contraction that affects the accretionary wedge, a narrow sector at the western termination of the Ionian Basin (i.e. the turbidite valley, see Gutscher et al., 2016 and Fig.1c for location) has not yet been overthrust by the compressional front of the Ionian Accretionary wedge. Rather, Plio-Quaternary extension is preserved in the area, where the narrow turbidite basin is deformed by a belt of extensional faults that nucleated at the foot of the MESC (Gambino et al., 2021). The turbidite basin is confined between the MESC in the West, and the NW-trending, dextral North Alfeo Fault to the East (NAF in Fig.1b, see Gutscher et al., 2016), which separates the extensional basin from the contractional domain of the Calabrian accretionary wedge (Fig.1b). Submarine canyons excavated in the MESC slope (Micallef et al., 2018, Fig.1c) reveal that the turbidite basin has been filled both by sediments discharged from the subaerial footwall-block of the Malta Escarpment, and also from the North according to sediment wave patterns (Gutscher et al., 2016). Active extensional deformation affecting the turbidite basin results in a system of normal faults that have been previously reported in literature (see Bianca et al., 1999; Argnani and Bonazzi, 2005; Monaco and Tortorici, 2007; Meschis et al., 2020). Recently, high-resolution seismic surveys in the area (Gutscher et al., 2016) and accurate tectono-stratigraphic interpretation (Gambino et al. 2021), have allowed the active deformation pattern affecting the northernmost sector of the MESC to be redefined. The latter is characterized by the occurrence of three main, E-dipping, and slightly oblique (right-lateral) fault segments (F1, F2, and F3 in Figs. 1c and 2) slicing mainly along the foot of the MESC bathymetric scarp. Further East, a narrow graben structure, associated with the main fault system, is found to longitudinally deform the turbidite valley, displacing both the section of Quaternary sediments and the seafloor itself.


## 3. Tectono-stratigraphic model

### 3.1. Seismo-stratigraphic setting

The seismo-stratigraphic setting was derived from a previous interpretation performed on the selected seismic profiles (see Gambino et al. 2021). Four main seismic units (Pre-MES, MES, PQ, and PQ2) were recognised according to well-defined bounding stratigraphic discontinuities (horizons S1, S2, S3 and, seafloor S4, see Fig.2). To better constrain the restoration with time, the PQ1 unit has been further subdivided in three sub-units (PQ1a, PQ1b, and PQ1c) according to the detected S3a and S3b bounding unconformities (Fig.2). Since no borehole data are available for the study area, lithologies and ages of the seismic units have been interpreted according to the available literature (see Gambino et al., 2021 and references therein) and summarized in Tab.1. The Pre-MES unit represents the backbone of the Malta Escarpment and has been interpreted as Meso-Cenozoic limestones and marls with sporadic volcanic and/or mud intrusions (Scandone et al., 1981; Catalano et al., 2001; Barreca, 2014). The MES unit has been interpreted as the Messinian sequence based on its seismic characters (high-reflectivity of the top-reflector, see Lofi et al., 2011; Camerlenghi et al., 2019; Micallef et al., 2019 and reference therein) and for its internal stratigraphy (Butler et al., 2015).The PQ1 unit (including its subunits PQ1a, PQ1b, and PQ1c) has been interpreted as a Pliocene sedimentary sequence since it correlates with coeval units described by Camerlenghi et al., (2019) and Micallef et al., (2018). According to these authors, the PQ1 subunits are interpreted as a sequence of siltstone (shale) and silty-sandstones, calc-lutites and marls. Finally, the PQ2 unit is interpreted as a Quaternary sequence given its seismic character and stratigraphic position. Moreover, its basal erosional surface, dated to 650 ka (Camerlenghi et al., 2019), suggests a correlation with the Middle-late Pleistocene calcarenitic sequence outcropping on-land (Servizio Geologico d'Italia, 2011).

### 3.2. Deformation Pattern

According to Gambino et al., (2021), reactivation of the MESC system is manifest by an array of seaward-dipping, NNW–SSE trending, extensional faults. The system extends offshore from Catania (Northern termination) to Siracusa (Southern termination) with a total length of ~60 km (Fig.1). The extensional belt includes three main faults (F1, F2, and F3) running close to the MESC lower slope, with a 3.5 km-wide graben structure further to the East bounded by the F4 and F5 faults (Fig. 2a). The F3 structure is the longest fault, reaching a length of ~ 56 km. The MESC fault activity has produced a cumulative vertical displacement of the seafloor of about 130 m (see Tab. 2a and b). The offset across faults generally increases with depth involving the entire Plio-Quaternary sequence and the Messinian top reflector (S2, Fig. 2). The estimated rate of fault activity ranges from 0.1 mm/yr during the Pliocene to ~ 0.4 mm/yr during the Pleistocene. However, based on the height of seafloor scarps, a vertical deformation rate of up to 10mm/yr was

estimated for the Holocene time interval along the F3 fault (see Gambino et al., 2021). This value is probably overestimated and could be the result of various factors affecting bathymetry (erosion, slope instability, etc.).

Farther to the east, the turbidite basin is bounded by a structural culmination (the so called 'uplifted area' of Argnani and Bonazzi, 2005, Fig.2a). It has been interpreted as a recent positive flower structure resulting from the propagation of the NW-SE trending dextral NAF (see Gutscher et al., 2016 and Fig.1 for location) or, alternatively, as a forced fold produced by the diapiric uprising of mantle-derived serpentinite material (Polonia et al., 2017). The structural culmination is deformed on its shallower portion by a set of high-angle active/recent faults (Fig. 2a) that have also been considered in the restoration process. The kinematics of these faults is related to the dextral strike-slip nature of NAF (Figs.1, 2a), which produces a cumulative normal component observed in seismic section (Cir-01 in Fig.2a). The active deformation pattern characterizing the investigated region is that of an extending domain where deformation appears to be currently accommodated by the activity of the F1, F2, and F3 faults.

## 4. Restoring the model

To back-deform the tectono-stratigraphic model (Fig. 2), a workflow encompassing several restoration methods (i.e. unloading of top units, decompaction of underlying units, isostatic adjustments, erosion restoration, structural restoration and unfolding of horizons), was adopted (see supplementary material). Due to the geometric and structural complexities, the tectono-stratigraphic model was simplified into four continuous blocks (see Schultz-Ela, 1992) separated by the F1, F2, and F3 faults (block model in Fig. 2-right panel). Block 1 represents the footwall of the F1 fault, Block 2 is both the F1 hanging-wall and the F2 footwall, Block 3 is the F2 footwall as well as the F3 hanging-wall and, lastly, Block 4 is the F3 hanging-wall. Fault displacement parameters (i.e. throw, heave, and slip) have been measured during the restoration and reported in Tab.2a (CIR-01 profile) and Tab.2b (P607 profile).

### 4.1. Restoration of the CIR-01 profile

Restoration of the CIR-01 profile involved 48 sequential steps that have included a preliminary tectono-stratigraphic interpretation and a time/depth conversion of seismic units. The most representative steps are shown in Fig.4 where the interpreted CIR-01profile has been restored by applying the proposed restoration workflow (see supplementary material).

After seismic interpretation (Step-01) and the time/depth conversion (Step-02), restoration started from the present-day structural configuration (Step-03). At this stage, Block 4 is deformed

by a graben related to the activity of the F4 and F5 opposite-dipping faults (see Fig. 2) and by other minor faults developed in the uplifted area to the east (see Fig. 2 for details). The graben represents the latest structure to have formed, (Gambino et al 2021) since the bounding faults show a constant offset with depth (from PQ1 downward). However, F5 forming the easternmost fault of the graben (Fig. 2a), shows displacement increasing with depth, indicating its older activity. For this reason, the F5 structure has been restored by several steps that adopt a "simple shear method" (see supplementary material).

During Step-05, the graben has been back-deformed by means of structural restoration applied to both F4 and the minor faults within the graben. At Step-06, the PQ2 unit is stripped-back and the lower units de-compacted accordingly. In Step-07, erosion of PQ1c has been considered in the restoring workflow. To gather information about the amount of eroded succession, the pattern of internal reflectors within the PQ1c unit has been analysed. The seismo-stratigraphic sequences observed in Block 1 and Block 4b can be considered as lacking erosion since no stratigraphic truncations have been detected. Conversely, parts of the PQ1c is missing in Block 2, Block 3 and Block 4a (Fig.3a). Accordingly, restoration of the S3 horizon (top of PQc1 unit) is therefore performed by considering the eroded stratigraphic portion and following the geometric pattern of the basal bed of PQ1c unit (the S3a horizon, Fig. 3b). Along Block 4a, patterns of internal reflectors indicate significant amounts of erosion with the PQ1c unit locally being only a third of the original stratigraphic thickness. Along Block 3, the reflector pattern is difficult to observe due to their chaotic setting, and erosion has been restored by considering the adjacent Blocks 2 and 4.

In Step-12, the constant with depth displacement of faults in the uplifted area (FU2, FU3, FU4, FU5 in Fig. 2a and Fig. 4) is restored in one step after the structural restoration of the S3 horizon. This indicates that the onset of faulting occurred after the deposition of the PQ1c unit. At this step, the cumulative extension accommodated by all the faults is ~127 m. In Step-13, unfolding is applied to the S3 horizon. Since no paleo-bathymetric data is available, unfolding was performed by considering a single horizontal datum for the entire seismic sequence (datum 1 in Fig.3d-1). The vertical deformation required to honour such a datum (up to 287m) is too great to be considered geologically consistent. Unfolding was then applied by using a horizontal datum (datum2 in Fig.3d-2) for units located within the turbidite basin (i.e. eastward of the F1 fault) whereas an inclined datum is maintained for units located on the slope (i.e. westward of the F1 fault). This choice is geologically consistent since part of the sediment source is in the MESC upslope (as evidenced by submarine canyons along the MESC slope, see Micallef et al., 2019) and a wedge deposition is expected at the base of the slope. The result of unfolding is shown in Fig.3d2 and Fig 4.

In Step-20, the PQ1c is unloaded from the section and lower units de-compacted, while at Step-27, faults are restored with respect to the S3b horizon and a total extension of ~205 m is achieved. In Step-29, all units are unfolded with respect to the S3b horizon. As for Step-13 described above, an inclined and a horizontal datum were adopted for the lower-slope and basin units, respectively. It is worth noting that unfolding of the units produced a decoupling (space in Fig. 4) between the lower-slope units (PQ1a, PQ1b and MES) and the Pre-Mes unit. The space reflects the concept of 'area conservation' (Chamberlin, 1910) that is required for 2D back restorations. We interpret this feature as being related to accommodation of sediments due to progressive loading. This interpretation could also explain the upward concavity at Step-03 of S3a, S3b, and S3 horizons located on the MESC lower-slope (Fig. 4).

At Step-35, the PQ1b unit is unloaded and lower units de-compacted, while in Step-42, faults are restored with respect to the S3a horizon (top of PQ1a unit). Restoration of the F5 fault led to an inconsistency on the undeformed S2 horizon, which resulted in it being higher in the hanging wall. Even though negligible, such a discrepancy could be the result of an incorrect picking of the S2 horizon.

### 4.2. Restoration of the P607 profile

The sequential restoration of the P607 profile involved 19 steps among which the salient ones are shown in Fig.5. After the time-to-depth conversion of the seismic profile (Step-05, Fig. 5), the PQ2 unit is unloaded and underlying units de-compacted (Step-06). As for other steps, in the presence of growth strata (see PQ2 unit at Step-05, Fig. 5) sediment unloading and decompaction of lower units follows the operation explained in Fig. 3c (see also supplementary material). Accordingly, different loading on underlying units (located in the footwall and hanging wall, respectively) due to regional and local load (i.e. increased near fault) are unloaded separately.

During Step-08, faults are restored. It is worth noting that, contrary to the CIR-01 profile, no erosional restoration has been performed to the PQ1c unit since the S3 horizon does not provide an indication of the amount of eroded sequence. This is possibly due to a paraconformity which hides the erosional nature of S3 surface (Fig. 2b). This aspect led to an overestimation of F1 throw (see Fig. 6 and section 5).

Unfolding is applied in Step-09. As for the CIR-01 seismic line, an inclined datum was used to unfold units formed on the lower-slope and a horizontal one to unfold units located in the adjacent turbidite basin. In Block 2, offset produced by the F2 fault on the S3b horizon (top of the PQ1b unit, see Fig. 3b) is not consistent with the extensional kinematics of the fault since the footwall is lower than the hanging wall. Moreover, the S3b horizon in Block 2 is bent downwards approaching

the F2 fault. Since bending is not observed in either the upper nor in the lower horizons, it could be the result of local erosion produced by slope instability. Hence, the S3a horizon has been restored (Step-10) using the lower S3b horizon as a reference template (Fig.3b).

In Step-10, erosion of PQ1b at block2 has been restored (see also Fig.3b), while in Step-12, the PQ1c unit is unloaded and underlying units de-compacted. Faults are restored in Step-13, and unfolding is applied to the S3b horizon in Step-14. In step-15, the PQ1b unit is unloaded and lower units de-compacted. It is notable that the F2 fault does not produce offset on lower units (PQ1a and MES), suggesting that this fault nucleated after the deposition of the PQ1a unit. In Step-16, faults are restored with respect to the S3a boundary, and at Step-17 unfolding is applied to the S3a horizon. The PQ1a unit has been stripped back and faults are restored with respect to the S2 horizon in Step-19.

### 4.3. *Fault displacement parameters and rate of deformation*

The results of the sequential restoration of each seismic profile permits us to investigate the vertical and horizontal deformation experienced by the investigated sector (i.e. including all the faults) and their contribution to the overall deformation by the MESC faults (F1, F2, and F3, see Tab. 2a and b for the CIR-01 and the P607 profiles, respectively). For each step in the restoration, displacement parameters (i.e. throw, heave, and slip) of all faults have been measured (Tab. 2) and plotted for each displaced unit (Fig. 6). Fault displacement parameters from unrestored seismic sections are also plotted for comparison (Fig. 6a-c). After the restoration process, the measured fault's throws along the CIR-01(Fig. 6b) and the P607 (Fig. 6d) profiles show a flattened trend compared to the unrestored sections, marking a significant reduction of the vertical offsets for each displaced horizon. In the CIR-01 profile, a reduction of the vertical displacement is observed for the MESC faults and it progressively increases further back in time. From the PQ1b unit (Middle Pliocene) to the present-day, the MESC faults (F1, F2, and F3) show a relatively flat throw trend with an average vertical displacement of about 50 m for each considered horizon (~25 m for the F2 and F3 faults, and ~75 m for the F1 structure, see Tab. 2a and Fig. 6b). The same trend and offset reduction are observed in the P607 profile except for the PQ1c unit that seems to have experienced up to 250 m of vertical displacement (Fig. 6d). Since the erosional surface at the base of the PQ1c unit is not clearly detectable in the P607 profile, the throw affecting the PQ1c top-horizon (S3 discontinuity) has not been restored relating to the eroded stratigraphic thickness. This limitation probably produced an overestimation of the throw value for the PQ1c unit. Considering that a decrease of about one half of the throw affecting the PQ1c unit was measured in the adjacent CIR-01 profile

after restoring the eroded sedimentary thickness, a more reliable throw in the order of ~100 m is inferred for the PQ1c unit also along the P607profile (see dashed black line in Fig. 6d).

The revised fault throws were then used to evaluate the vertical movement of the MESC faults overtime (Fig. 7a). During the considered time interval, faults vertically deform the seismic units at an average rate of 0.15 mm/yr (0.18 and 0.14 mm/yr for CIR-01 and P607 profiles respectively, Tabs.3a-b and Fig.7a). The maximum throw-rate value (0.4 in the CIR-01) is observed at the Lower-upper-Pliocene transition for MESC faults. During the Upper Pliocene-Pleistocene, throw-rates decrease and stabilize at 0.09 and 0.05 mm/yr for the P607 and CIR-01 profiles, respectively. To discriminate and separate the contribution of the MESC faults to the whole basin deformation (vertical and horizontal components), cumulative throw and heave of the MESC extensional system (F1, F2, and F3) have been compared with the total amount of recovered extension (whole extension in Tab.2a) achieved by back-deforming all the faults (Fig. 7). At the undeformed stage (see step 48 in Fig. 4), restoration of all faults results in ~ 800 m of total extension and ~640 m of total throw. At this stage, the MESC faults contribute 30% (258 m) of total extension and 40% (251m) of the achieved total throw. Both the vertical and horizontal component of total deformation (blue and red solid lines in Fig. 7b) decrease toward the present-day roughly correlating with the trend of the deformation components of the MESC faults (see blue and red dashed lines in Fig. 7b). This pattern suggests that in the older stage (MES-PQ1a transition), deformation was rather distributed in most of the faults detected in the tectono-stratigraphic model. The prevalence of the extensional component provides an insight on this incipient stage of deformation, with a probable diffuse extensional strain across the entire investigated sector. In the mature stage (i.e. moving towards the present-day), almost the entire deformation (i.e. the 97.48% of vertical component, see Tab.3a), is accommodated by the MESC faults indicating strain localization along these tectonic structures.


## 5. Discussion

The restoration sequence proposed here aims to better constrain the tectonic rates of faults slicing across the MESC by means of seismo-stratigraphic analysis and back restoration modelling. The identification of an erosively truncated unit (the PQ1c top-reflector) within the investigated sediment section, provides additional issues both in applying the restoration workflow and on the estimation of the vertical deformation rate affecting the investigated sector during the Quaternary. Nevertheless, the analysis of the PQ1c/PQ2 erosive truncation (dated at 650 ka, see Camerlenghi et al., 2019) along the CIR-01 profile (Fig.3a), provides an estimation of the amount of erosion experienced by the PQ1c top-reflector (S3 horizon). The reconstruction of the eroded PQ1c unit

reveals that up to about one third of its original thickness was eroded (Fig. 3a top-right). The maximum amount of erosion has been inferred at the depocenter of the turbidite basin (70 m, see block 4a in Fig.3a). Such an estimation was not possible in the P607 profile because of the nature of the para-conformity erosive truncation (see Fig. 2b). This issue produced an overestimation of the F1 throw (~250 m) affecting the PQ1c unit. However, according to the restored offset in the adjacent CIR-01 profile, the overestimation was corrected making the fault-throw curve for the P607 (Fig. 6d) consistent with the fault-throws achieved in the CIR-01 seismic line (Fig.6b). Restoration of the PQ1c original thickness necessitates a review of previously estimated vertical deformation of the MESC faults during the Quaternary (see Gambino et al., 2021, and Tab.2a). The F1 restored throw results in about only half of the unrestored one (i.e. from 146.20 m to 69.23 m in the CIR-01 profile see Tab. 2a). Vertical offset along the F2 structure is instead reduced by about one third (from 33.74 to 20.36 m, see Tab. 2a). Negligible reduction of the offset is observed for the F3 fault. The different offset reduction along the MESC faults is in line with the higher erosion rate expected along the hanging wall blocks.

Besides the F1 and the F3 tectonic structures, restoration of the F2 fault does not show vertical displacement for the PQ1a and MES units along the P607 profile (red line in Fig. 6d) and for the PQ1a unit along the CIR-01 profile (Fig. 6b). These data suggest that the F2 fault likely nucleated after deposition of the PQ1a unit and hence is later than the F1 and F3 structures (Lower Pliocene - see Fig. 6d and Step-15 in Fig. 5). Computer modelling allows us to derive information on the fault's throw and extension experienced by the whole investigated sector during the considered time-interval. In this context, a throw rate for the MESC faults is calculated considering the age of displaced surfaces in both seismic profiles (Fig. 7a). Since no well data are available, the age of the stratigraphic boundaries could be affected by uncertainties and, accordingly, a reliable estimation of the fault rate becomes rather challenging. The S2 surface (MES top-horizon) correlates with the upper Messinian limit and represents the only horizon whose age is well known from the literature (5.3 Ma, Camerlenghi et al., 2019; Lofi et al., 2011; Micallef et al., 2019). The PQ1 sediment package is Pliocene in age (see Gambino et al., 2021 and references therein) but uncertainties persist about the ages of its sub-units. Following this limitation, we propose age ranges based on the units' stratigraphic positions (see Tab.1).

A comparison between the total throw and extension (all faults, blue and red solid lines in Fig. 7b) and MESC related throw and extension (blue and red dashed lines in Fig. 7b) provides an insight into how deformation was modulated through time. Plotted values show that throw and extension produced by the activity of the MESC faults (F1, F2, and F3) have comparable values for each restoration step as expected by the mean dip-angle (45°) of the faults. Throws and extension

maintain roughly constant trends with a slight decrease from the Upper Messinian to the present-day. Conversely, throw and extension amounts related to the activity of all detected faults show high values during the Messinian-Lower Pliocene transition. This feature suggests that in the early stages, extensional deformation was diffuse and probably controlled all faults. In this time frame, MESC faults contributed only ~40% of the total throw and ~33% of the total extension (see the restoration Step-48 in Tab.3a). As deformation continues, total throw and extension decrease and, approaching the present day (PQ2 in Fig.7b and Tab.3a), the total throw affecting the area (97.48%) is largely accommodated by the MESC faults. Moreover, in the early deformation stage (from MES to PQ1b in Fig.7b) total extension (red solid line) is higher than the total vertical throw (blue solid line) suggesting that horizontal extension was the main component of deformation. Then, from PQ1b onwards, a change in the deformation style is observed with a predominant vertical component. This evidence allows us to infer that another deformation process, characterized by a major extensional component, worked simultaneously with the fault's activity in the early stage of deformation. This process is probably related to a diffuse extensional strain developed before fault nucleation or, alternatively, to ductile deformation in the underlying MES unit. In the final stage of the CIR-01 restoration (from Step-43 to Step-48 in Fig. 4), the S2 horizon (and related MES unit) remained strongly bent along Block 4. Considering the hyaline nature of the underlying MES unit and that no extensional fault can explain such bending, the S2 curvature is probably the result of a ductile deformation. Lateral escape of the plastic evaporites driven by the increased vertical load is invoked to explain the anomalous bending of the S2 horizon. Salt deformation cannot be restored by means of classical back restoration methods since salt typically assumes three-dimensional escape directions and dissolution (Rowan and Ratliff, 2012). Moreover, it is observed how salt migration due to sediment loading may produce similar effects of local subsidence and uplift (Rojo et al., 2020) which could explain the non-horizontal S2 horizon.

## 6. Conclusion

Sequential restoration was applied to a tectono-stratigraphic model derived from the interpretation of two high-resolution seismic profiles crossing the Malta Escarpment and related extensional basin offshore eastern Sicily. This allowed us to obtain a more reliable deformation rate for the investigated sector. Sediment unloading/decompaction along with horizon unfolding, and erosional restoration have proven powerful methods in re-interpretation/validation of previously interpreted seismic profiles, and in assessing fault activity and the rate of crustal extension affecting the area.

The main outcomes stemming from this study are summarized as follows:

- Fault displacement parameters derived from the restored seismic profiles indicate that the MESC faults maintain a roughly constant throw (about 150 m, see Fig. 7) for each restoration step. Estimated rates of deformation suggest that the MESC faults throw-rates have been modulated through time spanning from 0.09 to 0.40 mm/yr in the Pliocene, and from 0.05 to 0.09 mm/yr during the Pleistocene. Extensional rates are estimated at 0.06 to 0.31 mm/yr during the Pliocene, and from 0.03-0.08 mm/yr during the Pleistocene.

- Throw and extension achieved from all faults in the CIR-01 profile indicates that during the early stage (post-Messinian), a diffuse extensional strain affected the investigated sector. This is evidenced by the significant difference between MESC faults deformation (i.e. extension and throw in Fig.7b) and the whole deformation (whole extension and whole throw in Fig.7b). In this context, the MESC faults contributed a third of total extension and throw during the early deformation stage (Lower Pliocene). As deformation continued, the total deformation (whole extension and whole throw in Fig.7b) decreases and is taken up almost entirely by the MESC faults (Fig.7b). At the present-day, MESC faults accommodate ~97.5% of the total vertical deformation as well as most of the Quaternary extensional deformation affecting the investigated sector.

- Data analysis also suggests that in the early stages of deformation (MES/PQ1a transition, Fig. 7b), the extensional component of deformation prevailed over the vertical one. This suggest that another process was active at that time along with the MESC faults, probably still at their incipient stage. This extension may be related to ductile deformation within the MES unit.

- Uncertainties persist about the present-day rate of deformation. The high rate of vertical deformation affecting the MESC faults during the Holocene (3-7 mm/yr, see Gambino et al., 2021), is in contrast with the relatively low fault deformation rate (up to 0.4 mm/yr) estimated for the Pliocene sedimentary section. This would imply that a significant acceleration in the (tectonic, non-tectonic?) deformation probably occurred along faults with strain localization and reduction in frictional properties at fault cores.

Structural interpretation and back-restoration along two high-resolution seismic profiles crossing the Malta Escarpment provides insights that allow us to assess fault deformation rates along the Western Ionian Basin, the most seismically hazardous area of the central Mediterranean. Back-deformation of a geologically constrained tectono-stratigraphic model points to a revision of the throw-rates for the MESC faults. The vertical and horizontal deformation rate calculated over time reveals that the investigated sector is a low deforming area. We estimate a more reliable vertical offset that is about 2/3 of that measured in the unrestored sections (e.g. Step-03 for the CIR-01 and

Step-05 for the P607 profile, respectively) with significant seismotectonic implications. The workflow presented here allows new insights into basin deformation; in particular, two different processes which contributed to the tectonic evolution of the basin have been quantitatively discriminated. Moreover, the workflow has shown itself to be a powerful approach for analysis of basin deformation which can be applied to a wide range of tectonic contexts (extensional, contractional or composite).

# References

Airy, G. B. (1855). On the computation of the effect of the attraction of mountain- masses, as disturbing the apparent astronomical latitude of stations of geodetic surveys. Philosophical Transactions of the Royal Society, 145, 101–104.

Amato, A., Azzara, R., Basili, A., Chiarabba, C., Cocco, M., Di Bona, M., & Selvaggi, G., (1995). Main shock and aftershocks of the December 13, 1990, Eastern Sicily earthquake. Annali di Geofisica, vol. 37 (2) p.255-266.

Argnani, A., Armigliato, A., Pagnoni, G., Zaniboni, F., Tinti, S., & Bonazzi, C., (2012). Active tectonics along the submarine slope of south-eastern sicily and the source of the 11 january 1693 earthquake and tsunami. Nat. Hazards Earth Syst. Sci. 12 (5), 1311–1319. doi:10.5194/nhess-12-1311-2012.

Argnani, A., & Bonazzi, C. (2005). Malta Escarpment fault zone offshore eastern Sicily: Pliocene-Quaternary tectonic evolution based on new multichannel seismic data. Tectonics 24, TC4009. doi:10.1029/2004TC001656.

Azzaro, R., & Barbano, M. S. (2000). Analysis of the seismicity of southeastern Sicily: a proposed tectonic interpretation. Ann. Geofisc. 43 (1), 171–188. doi:10.4401/ag-3628.

Baldwin, B., & Butler, C. O. (1985). Compaction curves. AAPG bulletin, 69(4), 622-626.

Barnett, Jim A. M., John Mortimer, John H. Rippon, John J. Walsh, & Juan Watterson. (1987). Displacement geometry in the volume containing a single normal fault. American Association of Petroleum Geologists Bulletin 71 (8): 925-937.

Bianca, M., Monaco, C., Tortorici, L., & Cernobori, L. (1999). Quaternary normal faulting in southeastern Sicily (Italy): a seismic source for the 1693 large earthquake. Geophys. J. Int. 139, 370–394. doi:10.1046/j.1365-246x.1999.00942.x

Bonforte, A., Catalano, S., Maniscalco, R., Pavano, F., Romagnoli, G., Sturiale, G., & Tortorici, G. (2015). Geological and geodetic constraints on the active deformation along the northern margin of the hyblean plateau (SE sicily). Tectonophysics, 640, 80-89. doi:10.1016/j.tecto.2014.11.024.

Boyer, S.E., & Elliot, D., (1982). Thrust systems. Bulllet. Am. Assoc. Petrol. Geol. 66, 1196e1230.

Brewer, R. C., & Kenyon, P. M., (1996). Balancing Salt Dome Uplift and Withdrawal Basin Subsidence in Cross-Section. *Journal of StructuralGeology* 18 (4): 493-504. doi:10.1016/0191-8141(95)00098-X

Butler, R. W. H., Lickorish, W. H., Grasso, M., Pedley, H. M., & Ramberti, L. (1995). Tectonics and sequence stratigraphy in messinian basins, sicily: Constraints on the initiation and termination of the mediterranean salinity crisis. Geological Society of America Bulletin, 107(4), 425-439. doi:10.1130/0016-7606(1995)107<0425:TASSIM>2.3.CO;2

Butler, R. W. H., Maniscalco, R., Sturiale, G., & Grasso, M. (2015). Stratigraphic variations control deformation patterns in evaporite basins: Messinian examples, onshore and offshore Sicily (Italy). J. Geol. Soc. 172, 113–124. doi:10.1144/jgs2014-024

Camerlenghi, A., Del Ben, A., Hübscher, C., Forlin, E., Geletti, R., Brancatelli, G., Micallef, A., Saule, M., & Facchin, L. (2019). Seismic markers of the messinian salinity crisis in the deep ionian basin. *Basin Research, 32*(4), 716-738. doi:10.1111/bre.12392

Catalano, R., Doglioni, C., & Merlini, S. (2001). On the mesozoic ionian basin. Geophysical Journal International, 144(1), 49-64. doi:10.1046/j.0956-540X.2000.01287.x

Catalano, R., Valenti, V., Albanese, C., Accaino, F., Sulli, A., Tinivella, U., et al. (2013). Sicily's fold-thrust belt and slab roll-back: The SI.RI.PRO. seismic crustal transect. Journal of the Geological Society, 170(3), 451-464. doi:10.1144/jgs2012-099

Chamot-Rooke, N., Rangin, C., & Le Pichon, X., (2005). DOTMED–Deep Offshore Tectonics of the Mediterranean: a synthesis of deep marine data ineastern Mediterranean. Mémoirede la Société géologique de France & AmericanAssociation of Petroleum Geologists . special number, 177: 64 pp, 9 maps withCD-ROM.

Dahlstrom, C.D.A., (1969). Balanced cross sections. Canadian Journal of Earth Sciences

6, 743–757.

Dellong, D., Klingelhoefer, F., Kopp, H., Graindorge, D., Margheriti, L., Moretti, M., et al. (2018). Crustal structure of the Ionian basin and eastern Sicily margin: Results froma wide-angle seismic survey. Journal of Geophysical Research: Solid Earth, 123, 2090–2114. https://doi.org/10.1002/2017JB015312

Dickinson, G., (1953). Geological aspects of abnormal reservoir pressures in Gulf Coast, Louisiana: AAPG Bulletin, v.37, p. 410–432.

Egan, S.S., Buddin, T.S., Kane, S.J., & Williams, G.D., (1996). Three-dimensional modeling and visualization in structural geology: new techniques for the restoration and balancing of volumes. In: Proceedings of the 1996 Geoscience Information Group Conference on Geological Visualization, Electronic Geology 1, pp. 67–82. Paper 7.

Elliott, D., (1983). The construction of balanced cross sections. Journal of Structural Geology 5, 101.

Frizon de Lamotte, D., C. Raulin, N. Mouchot, J.- C. Wrobel- Daveau, C. Blanpied, & J.- C. Ringenbach (2011), The southernmost margin of the Tethys realm during the Mesozoic and Cenozoic: Initial geometry and timing of the inversion processes, Tectonics, 30, TC3002, doi:10.1029/2010TC002691.

Galadini, F., & Galli, P. (2000). Active tectonics in the central appennines (italy) - input data for seismic hazard assessment. Natural Hazards, 22(3), 225-268. doi:10.1023/A:1008149531980

Gallais, F., Gutscher, M.-A., Graindorge, D., Chamot-Rooke, N., & Klaeschen, D. (2011). AMiocene tectonic inversion in the Ionian Sea (central Mediterranean): evidence from multichannel seismic data. J. Geophys. Res. 116, B12108. doi:10.1029/2011JB008505

Gallais, F., M. -A Gutscher, D. Klaeschen, & D. Graindorge. 2012. Two-Stage Growth of the Calabrian Accretionary Wedge in the Ionian Sea (Central Mediterranean): Constraints from Depth-Migrated Multichannel Seismic Data. *Marine Geology* 326-328: 28-45. doi:10.1016/j.margeo.2012.08.006.

Ge, H., Jackson, M.P., & Vendeville, B.C., (1997). Kinematics and dynamics of salt tectonics driven by progradation: AAPG Bulletin, 81, 398–423.

Gibbs, A.D., (1983). Balanced cross-section construction from seismic sections in areas of extensional tectonics. Journal of Structural Geology 5, 153–160.

Gibbs, A.D., (1984). Structural evolution of extensional basin margins, vol. 141. Journal of the Geological Society, London. 609–620.

Gratier, J.-P., Guiller, B., Delorme, A., & Odonne, F., (1991). Restoration and balance of a folded and faulted surface by best-fitting of finite elements: principle and applications. Journal of Structural Geology 13, 111–115.

Groshong Jr., R.H., (1990). Unique determination of normal fault shape from hanging wall bed geometry in detached half grabens. Eclogae Geol. Helvetiae 83, 455e471.

Groshong Jr., R.H., Bond, C.E., Gibbs, A., Ratcliff, R., & Wiltschko, D., (2012). Preface: structural balancing at the start of the 21st century: 100 years since Cham- berlin. J. Struct. Geol. 41, 1e5.

Gross, F., Krastel, S., Geersen, J., Hinrich, B. J., Ridente, D., Chiocci, F. L., et al. (2016). The limits of seaward spreading and slope instability at the continental margin offshore Mt. Etna, imaged by high-resolution 2D seismic data. Tectonophysics 667, 63–76. doi:10.10164/j.tecto.2015.11.011

Hossack, J.R., (1979). The use of balanced cross sections in the calculation of orogenic contraction: a review. J. Geol. Soc. Lond. 136, 705e711.

Jackson, M. P. A., & Talbot, C. J. (1991). A glossary of salt tectonics: Bureau of Economic Geology. Austin, TX: University of Texas at Austin.

Kokinou, E., Vafidis, A., Loucogiannakis, M., & Louis, I. (2013). Deep seismic imaging and velocity estimation in Ionian Sea. J. Balkan Geophys. Soc. 6 (2), 100–116.

Laurent G., Caumon G., Bouziat A., & Jessell M (2013). A parametric method to model 3D displacements around faults with volumetric vector fields. Tectonophysics, 590, pp.83-93. ff10.1016/j.tecto.2013.01.015ff. ffhal-01301478f

Le Meur, D. (1997). Etudegéophysique de la structure profonde et de la tectoniqueactive de la partieoccidentale de la Ride Méditerranéenne [Ph.D. thesis]. Paris (FR): University of Paris XI.

Maesano, F. E., Tiberti, M. M., & Basili, R. (2017). The Calabrian Arc: three-dimensional modelling of the subduction interface. Sci. Rep. 7, 8887. doi:10.1038/s41598-017-09074-8

Milia, A., & Torrente, M. M., (2018). Extensional Messinian basins in the Central Mediterranean (Calabria, Italy): new stratigraphic and tectonic insights. Oil & Gas Science and Technology – Revue d'IFP Energies nouvelles, InstitutFrançais du Pétrole, 73, pp.45. 10.2516/ogst/2018040. hal-01902842

Micallef, A., Camerlenghi, A., Georgiopoulou, A., Garcia-Castellanos, D., Gutscher, M.-A., Lo Iacono, C., et al. (2019). Geomorphic evolution of the Malta Escarpment and implications for the Messinian evaporative drawdown in the eastern Mediterranean Sea. Geomorphology 327, 264–283. doi:10.1016/j.geomorph.2018.11.012

Minelli, L., & Faccenna, C., (2010). Evolution of the Calabrian Accretionary wedge (Central Mediterranean). Tectonics, 29 (4), 1-21. http://dx.doi.org/10.1029/2009TC002562.

Musumeci, C., L. Scarfì, M. Palano, & D. Patanè. (2014). "Foreland Segmentation Along an Active Convergent Margin: New Constraints in Southeastern Sicily (Italy) from Seismic and Geodetic Observations." *Tectonophysics* 630 (C): 137-149. doi:10.1016/j.tecto.2014.05.017.

Nixon, C. W., Sanderson, D. J., Dee, S. J., Bull, J. M., Humphreys, R. J., & Swanson, M. H. (2014). Fault interactions and reactivation within a normal-fault network at milne point, alaska. AAPG Bulletin, 98(10), 2081-2107. doi:10.1306/04301413177

Palano, M., Ferranti, L., Monaco, C., Mattia, M., Aloisi, M., Bruno, V., et al. (2012). "GPS Velocity and Strain Fields in Sicily and Southern Calabria, Italy: Updated Geodetic Constraints on Tectonic Block Interaction in the Central Mediterranean." *Rendiconti Online SocietaGeologicaItaliana* 21 (PART 1): 235-237

Peel, F. J. (2014a). The Engines of Gravity-Driven Movement on Passive Margins: Quantifying the Relative Contribution of Spreading Vs. Gravity Sliding Mechanisms.*Tectonophysics* 633 (1): 126-142. doi:10.1016/j.tecto.2014.06.023.

Peel, F. J. (2014b). How do Salt Withdrawal Minibasins Form? Insights from Forward Modelling, and Implications for Hydrocarbon Migration. *Tectonophysics* 630 (C): 222-235. doi:10.1016/j.tecto.2014.05.027.

Piatanesi, A., & Tinti, S. (1998). A revision of the 1693 eastern Sicily earthquake and tsunami. J. Geophys. Res. Solid Earth 103 (B2), 2749–2758. doi:10.1029/97JB03403.

Pizzi, A., Calamita, F., Coltorti, M., & Pieruccini, P. (2002). Quaternary normal faults, intramontane basins and seismicity in the umbria-marche-abruzziapennine ridge (italy): Contribution of neotectonic analysis to seismic hazard assessment. Bollettino Della SocietaGeologicaItaliana, 1(2), 923-929.

Rojo, L. A., Koyi, H., Cardozo, N., & Escalona, A. (2020). Salt tectonics in salt-bearing rift basins: Progradational loading vs extension. Journal of Structural Geology, 141 doi:10.1016/j.jsg.2020.104193

Rowan & Ratliff (2012). Cross-section restoration of salt-related deformation: Best practices and potential pitfalls. Journal of Structural Geology 41 (2012) 24-37.

Schultz-Ela, D.D., (1992). Restoration of cross-sections to constrain deformation processes of extensional terranes. Mar. Petrol. Geol. 9, 372e388.

Sclater, J. G., & Christie, P. A. (1980). Continental stretching: An explanation of the post- Mid- Cretaceous subsidence of the central North Sea Basin. Journal of Geophysical Research: Solid Earth, 85(B7), 3711-3739.

Stemberk, J., Moro, G. D., Stemberk, J., Blahůt, J., Coubal, M., Košťák, B., et al. (2019). Strain monitoring of active faults in the central apennines (italy) during the period 2002–2017. Tectonophysics, 750, 22-35. doi:10.1016/j.tecto.2018.10.033

Suppe, J., (1983). Geometry and kinematics of fault-bend folding. Am. J. Sci. 283, 684e721.

White, N.J., Jackson, J.A., & McKenzie, D.P., (1986). The relationship between the geometry of normal faults and that of sedimentary layers in their hanging walls. J. Struct. Geol. 8, 897e910.

## Figure captions

**Fig.1** - a) Simplified tectonic setting of Sicily and the Western Ionian Basin. b) Main tectonic structures in the study area with the F1, F2, and F3 faults representing the focus of this work. c) Location of 'turbidite valley' and the analyzed seismic profiles (blue lines). Solid lines are the CIR-01 and P607 seismic profiles discussed in the text, dashed lines are other seismic profiles from Gambino et al., (2021). White arrows indicate the direction of sediment supply.

**Fig. 2** - Tectono-stratigraphic models used for back-restoration. a) CIR-01 profile with the identification of three main sectors: MESC slope, turbidite basin and uplifted area. The uplifted area corresponds with the North Alfeo Fault system (NAF – Gutscher et al., 2016). b) P607 profile with the MESC slope turbidite basin. For both profiles, the schematic block model used for the restoration process is reported.

**Fig. 3 -** Main restoration steps. a) Restoration of erosion of the PQ1c unit (CIR-01 profile). Internal reflectors of Block 4b have been considered as the complete seismo-stratigraphic sequence. Accordingly, missing reflectors of Blocks 2, 3 and 4a provide an indication of the amount of erosion. b) Restoration of erosion of the PQ1b unit (P607 profile). S3b horizon (top of PQ1b) shows local erosion (due to slope instability) highlighted by footwall/hangingwall offset. Restoration has

been performed using the lower unit top reflector (S3a horizon) as a template. c) Unloading of the upper unit and decompaction of underlying ones. For units showing across-fault thickness variation (growth-strata) we considered a regional load acting on both the footwall and hangingwall of the considered fault, and a local load acting only on the hangingwall. As a result, different decompactions of lower units is applied to the footwall and hangingwall. d) Unfolding of seismic units. Two data have been considered since no paleo-bathymetric datum is available. Datum 2 (which is horizontal in the turbidite basin and inclined on the slope) has been chosen since it is geologically reliable (see text for description).

**Fig. 4** – Restoration sequence of CIR-01 profile. Bottom- right represents the present-day setting. In every restoration cycle, structural restoration is performed, and the related amount of extension is reported. At the end of each cycle, the inferred age is reported.

**Fig. 5** – Restoration sequence of the P607 profile. The present-day setting is shown in the bottom-right. In every restoration cycle, structural restoration is performed, and the related amount of extension is reported. At the end of each cycle, the inferred age is reported.

**Fig. 6** – Throws measured on tectono-stratigraphic models before (a, c) and after (b, d) restoration. In the time range axis, the units on which throws are measured are reported. For the restored diagrams (b, d) throws are measured before the structural restoration steps. When the considered unit represents the top unit of the sequence, the relative step numbers (related to Figs. 4 and 5) are reported above.

**Fig.7** - a) Cumulative throw-rate of F1, F2 and F3 (MESC faults) relative to CIR-01 (blue line) and P607 (red line). Every value is relative to the time interval between the seismic units reported (inferred ages are reported in Tab.1. b) Throws (blue lines) and extension (red lines) parameters achieved from the restoration of the CIR-01 profile. Dotted lines are relative to MESC faults parameters and solid lines are relative to the cumulative parameters of all faults within the seismic profile.

**Tab. 1** – Physical parameters attributed to the detected seismic units used for back restoration. Ages, lithologies and seismic velocities are based on literature data (see Gambino et al., 2021 and reference therein).

**Tab. 2** – Results achieved by means of the back restoration process (blue highlighted values are post-calculated). a) Data related to the restoration of the CIR-01 profile; b) Data related to the restoration of the P607 profile.

**Tab. 3** – Main results of back restoration (throws and extensions) and data elaboration (rates) of CIR-01 (a) and P607 (b).

Fig.1

Fig.2

Horizons: — S4 — S3 — S3b — S3a — S2 — S1

Seismic Units: PQ2 | PQ1c | PQ1b | PQ1a | MES | Pre-MES

Quaternary | Pliocene | Messinian | Pre-Messinian | Time line

Fig.3

**WSW** — **ENE**

Messinian/Pliocene 5.3 Ma

Step 48

Extension 784,3m

**WSW** — **ENE**

Lower Pliocene 4-5 Ma

Step 43

**WSW** — **ENE**

Step 42

Extension 368,8m

**WSW** — **ENE**

Step 35

**WSW** — **ENE**

Upper Pliocene ≈ 3.6 Ma

Step 29

**WSW** — **ENE**

Step 27

Extension 206m

**WSW** — **ENE**

Step 20

**WSW** — **ENE**

Pliocene/Pleistocene 2.58 Ma

Step 13

**WSW** — **ENE**

Step 12

Extension 126,8m

**WSW** — **ENE**

Step 07

**WSW** — **ENE**

Step 06

**WSW** — **ENE**

Step 05

**WSW** — **ENE**

Step 03

F1  F2  F3

0  1  2 km

-Unrestored Length

**Cir-01**

Horizons  Seismic Units

S4 — PQ2
S3 — PQ1c
S3b — PQ1b
S3a — PQ1a
S2 — MES
S1 — Pre-MES

Block1  Block2  Block3  Block4
F1  F2  F3  F4  F5

Block Model

Fig.4

**p607**

Messinian/Pliocene 5.3 Ma

Step19 — F1, F2, F3 — Extension 506,4m

Step12 — F1, F2, F3

Lower Pliocene 4-5 Ma

Step17 — F1, F2, F3

Step10 — F1, F2, F3

Step16 — F1, F2, F3 — Extension 342,0m

Pliocene/Pleistocene 2.58 Ma

Step09 — F1, F2, F3

Step15 — F1, F2, F3

Step08 — F1, F2, F3 — Extension 158,0m

Upper Pliocene ≈ 3.6 Ma

Step14 — F1, F2, F3

Step06 — F1, F2, F3

Step13 — F1, F2, F3 — Extension 297,5m

Step05 — F1, F2, F3

Unrestored Length

Horizons
S4
S3
S3b
S3a
S2
S1

Seismic Units
PQ2
PQ1c
PQ1b
PQ1a
MES
Pre-MES

Block Model

Block1 — Block2 — Block3 — Block4

F1 — F2 — F3

Fig.5

Fig.6



Fig.7

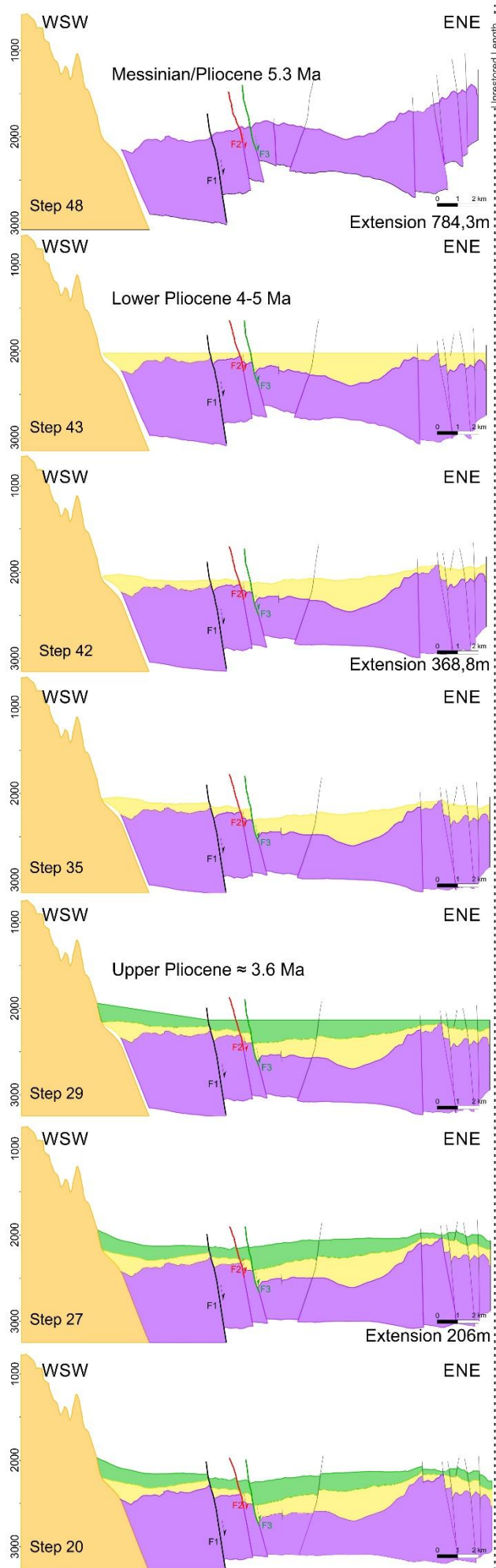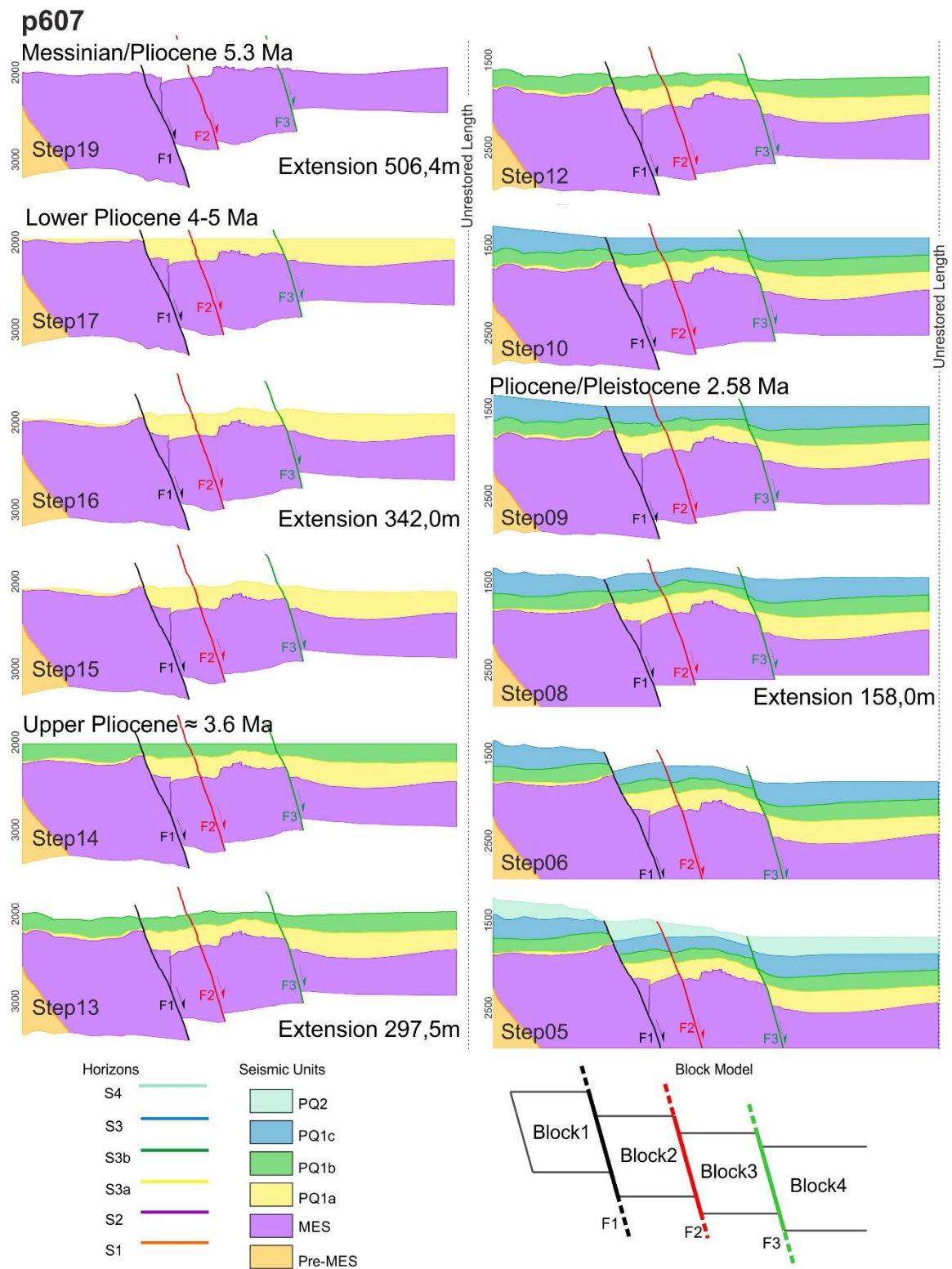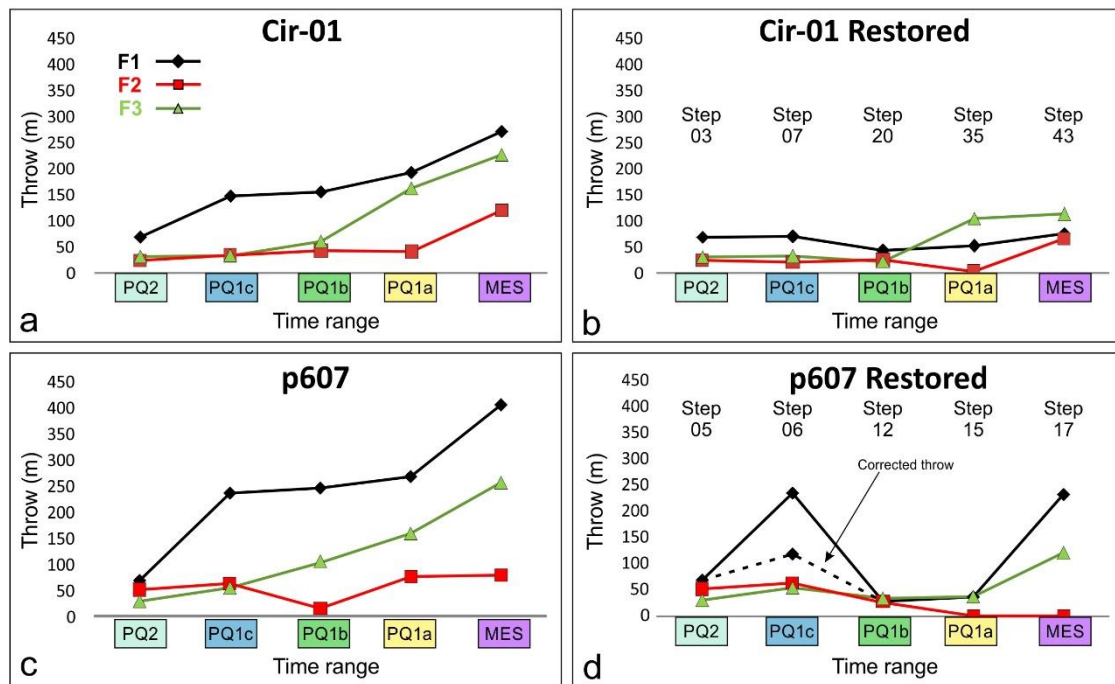| Seismic Unit | Age | Age (Ma) | Lithology | SeismicVelocity (m/s) | Surface porosity | Density (km/m³) | Depth Coeff. (km⁻¹) |
|---|---|---|---|---|---|---|---|
| PQ2 | Quaternary | 2.58-0.012 | Silty-sandstones | 1760 | 0.4 | 2700 | 0.39 |
| PQ1c | Upper Pliocene | 3.6-2.58 | Silty-sandstones | 2280 | 0.4 | 2700 | 0.39 |
| PQ1b | Upper/Lower Pliocene | 4.0-3.6 | Silty-sandstones | 2280 | 0.4 | 2700 | 0.39 |
| PQ1a | Lower Pliocene | 5.3-4.0 | Silty-sandstones | 2280 | 0.4 | 2700 | 0.39 |
| MES | Messinian | 7.2-5.3 | Evaporites | 4000 | 0 | 2200 | 0.00 |
| Pre-MES | Pre-Messinian | > 7.2 | Limestones | 3250 | 0.7 | 2700 | 0.71 |

Tab 1

| Total Throw | F1 Heave | F1 Slip | F1 Throw | F2 Heave | F2 Slip | F2 Throw | Heave |
|---|---|---|---|---|---|---|---|
| 23.80 | 50.72 |  | 68.30 | 27.40 |  | 24.10 | 26.79 |
| 70.94 | 77.75 | 165.66 | 146.20 | 54.92 | 64.57 | 33.74 | 16.97 |
| 47.78 | 142.26 | 211.89 | 153.89 | 44.59 | 61.43 | 42.15 | 46.93 |
| 10.45 | 222.64 | 295.11 | 190.95 | 53.84 | 67.41 | 40.38 | 114.89 |
| 115.07 | 283.69 | 392.69 | 268.79 | 109.95 | 165.89 | 119.13 | 282.63 |
| 90.89 | 36.63 | 78.40 | 69.23 | 26.27 | 33.24 | 20.36 | 20.22 |
| 56.96 | 109.50 | 168.31 | 125.34 | 45.16 | 63.56 | 44.61 | 46.29 |
| 63.03 | 222.66 | 294.86 | 190.56 | 48.77 | 61.59 | 37.48 | 117.44 |
| 152.65 | 283.69 | 392.95 | 268.89 | 109.93 | 166.68 | 120.15 | 282.63 |
| 96.80 | 25.77 | 49.76 | 42.54 | 21.47 | 32.67 | 24.58 | 16.03 |
| 02.28 | 107.87 | 149.11 | 101.34 | 28.66 | 37.46 | 24.12 | 81.40 |
| 14.91 | 191.87 | 255.50 | 166.65 | 90.01 | 133.96 | 94.37 | 238.54 |
| 59.38 | 56.37 | 77.67 | 51.62 | 3.32 | 4.38 | 2.86 | 62.75 |
| 14.65 | 145.92 | 189.58 | 120.91 | 74.41 | 106.64 | 71.13 | 207.08 |
| 44.62 | 85.61 | 114.38 | 75.77 | 84.75 | 109.41 | 64.32 | 87.93 |

Tab.2a

| Throw | F2 Heave | F2 Slip | F2 Throw | F3 Heave | F3 Slip | F3 Throw | F1 |
|---|---|---|---|---|---|---|---|
| 68.20 | 38.86 |  | 50.40 | 22.94 |  | 29.90 | 69.89 |
| 235.63 | 48.56 | 78.66 | 61.84 | 35.30 | 65.73 | 55.39 | 120.72 |
| 245.36 | 11.84 | 19.52 | 15.52 | 71.29 | 128.89 | 105.88 | 210.04 |
| 267.23 | 56.84 | 93.55 | 74.30 | 156.50 | 222.85 | 158.46 | 244.05 |
| 404.69 | 73.33 | 106.33 | 76.92 | 155.07 | 300.23 | 254.85 | 429.05 |
| 231.69 | 48.56 | 78.26 | 61.31 | 35.24 | 63.99 | 53.36 | 118.71 |
| 248.34 | 11.84 | 20.47 | 16.70 | 71.28 | 134.23 | 112.14 | 210.02 |
| 268.87 | 56.84 | 97.10 | 78.73 | 156.49 | 228.19 | 165.87 | 244.06 |
| 407.22 | 73.33 | 106.81 | 77.59 | 155.11 | 300.85 | 255.11 | 429.05 |
| 30.53 | 44.05 | 51.46 | 26.18 | 23.17 | 41.63 | 34.55 | 22.64 |
| 82.55 | 15.70 | 21.81 | 15.14 | 72.57 | 103.59 | 73.92 | 47.28 |
| 254.60 | 16.31 | 27.33 | 21.93 | 103.64 | 192.26 | 159.42 | 190.18 |
| 36.56 | 0.00 | 0.00 | 0.00 | 45.29 | 58.28 | 36.56 | 45.29 |
| 229.57 | 0.00 | 0.00 | 0.00 | 87.86 | 150.49 | 119.50 | 170.75 |
| 183.50 | 0.00 | 0.00 | 0.00 | 62.30 | 91.40 | 66.40 | 132.80 |

Tab.2b

| Cir-01 | | | | | | | | | | |
|---|---|---|---|---|---|---|---|---|---|---|
| Step | Unit | Total Throw | MESC Throw | % Throw | MESC throw rate | Total Extension | MESC Extension | % Extension | Total Ext. Rate | MESC Ext. rate |
| 03 | PQ2 | 127.00 | 123.80 | 97.48 | 12.38 | | 104.92 | | | 10.49 |
| 07 -12 | PQ1c | 190.89 | 121.51 | 63.65 | 0.05 | 126.80 | 83.12 | 65.55 | 0.05 | 0.03 |
| 20 - 27 | PQ1b | 196.80 | 89.73 | 45.59 | 0.09 | 206.00 | 63.27 | 30.71 | 0.21 | 0.06 |
| 35 - 42 | PQ1a | 259.38 | 158.27 | 61.02 | 0.40 | 368.80 | 122.44 | 33.20 | 0.92 | 0.31 |
| 43 - 48 | MES | 644.62 | 251.62 | 39.03 | 0.19 | 784.30 | 258.29 | 32.93 | 0.60 | 0.20 |

Tab.3a

| p607 | | | | | |
|---|---|---|---|---|---|
| Step | Unit | Throw | MESC Throwrate | MESC Extension | MESC Ext. rate |
| 05 | PQ2 | 148.50 | 14.85 | 131.69 | 13.17 |
| 06 - 08 | PQ1c | 230.52 | 0.09 | 202.51 | 0.08 |
| 12 - 13 | PQ1b | 91.26 | 0.09 | 89.86 | 0.09 |
| 15 - 16 | PQ1a | 73.12 | 0.18 | 90.57 | 0.23 |
| 17 - 19 | MES | 249.90 | 0.19 | 195.10 | 0.15 |

Tab.3b